

Building a Virtual Weakly-Compressible Wind Tunnel Testing Facility: Supplementary Material

CHAOYANG LYU, ShanghaiTech University / SIMIT / UCAS, China
 KAI BAI, ShanghaiTech University / AEROC AE Digital Ltd., China
 YIHENG WU, ShanghaiTech University, China
 MATHIEU DESBRUN, Inria / Ecole Polytechnique, France
 CHANGXI ZHENG, Tencent Pixel Lab / Columbia University, USA
 XIAOPEI LIU, ShanghaiTech University, China

This supplementary document is meant to complement the ACM SIGGRAPH 2023 paper [Lyu et al. 2023].

1 DERIVATION OF ENTROPY OPTIMIZATION ON CUMULANTS

As described in our main paper, the entropy function in LBM is typically defined as

$$H(\mathbf{f}) = - \sum_i f_i \ln \left(\frac{f_i}{\omega_i} \right), \quad (1)$$

where ω_i is the weight of the corresponding discretized velocity \mathbf{c}_i . We follow the work of [Kramer et al. 2019] and adopt a quadratic approximation of the entropy function:

$$\tilde{H}(\mathbf{f}) = - \sum_i \left(\frac{f_i^2}{\omega_i} - f_i \right) = \rho - \sum_i \frac{f_i^2}{\omega_i}, \quad (2)$$

which is referred to as the *pseudoentropy* function. This function is a Taylor expansion of $H(\mathbf{f})$ from Eq. (1) at the global equilibrium $f_i^{\text{eq}}(\rho = 1, \mathbf{u} = 0) = \omega_i$. The advantage of using a pseudoentropy function is that it provides a simple and explicit concave function to maximize. While [Kramer et al. 2019] provides a derivation to maximize pseudoentropy function for MRT, the assumption is made that the moment transformation must be linear, which is not the case for the cumulant collision operator: a cumulant transformation is nonlinear for cumulants of order $n \geq 4$. So here we derive pseudoentropy maximization for our cumulant collision model.

We set $\mathbf{k}_l = \{k_l, l \in \mathcal{L}\}$ as the cumulants up to order 3, since their relaxation rates are either fixed or optimized as in [Geier et al. 2017]. We can then define the rest of the cumulants, which are of orders 4 to 6, as $\mathbf{k} = \{k_h, h \in \mathcal{H}\}$. The pseudoentropy maximization can then be formulated as

$$\mathbf{f}^* = \arg \max_{\mathbf{k}} \tilde{H}(\mathbf{f}). \quad (3)$$

The difference between a central moment m_i and a cumulant k_i is denoted as r_i :

$$r_i = m_i - k_i. \quad (4)$$

Authors' addresses: C. Lyu, K. Bai, Y. Wu, X. Liu: School of Information Science and Technology (Shanghai Engineering Research Center of Intelligent Vision and Imaging) of ShanghaiTech University, Shanghai, China; C. Lyu is also affiliated with the Shanghai Institute of Microsystem and Information Technology (SIMIT) and the University of the Chinese Academy of Sciences (UCAS); K. Bai is now at the Aerocae Digital Ltd., Beijing, China; M. Desbrun: Inria Saclay / LIX, Institut Polytechnique de Paris, Palaiseau, France; C. Zheng: Tencent Pixel Lab / Columbia University, New York City, USA .

Then we can formulate f_i as

$$f_i = \sum_{l \in \mathcal{L}} t_{il} m_l + \sum_{h \in \mathcal{H}} t_{ih} m_h \quad (5)$$

$$= \sum_{l \in \mathcal{L}} t_{il} (k_l + r_l) + \sum_{h \in \mathcal{H}} t_{ih} (k_h + r_h). \quad (6)$$

with $T = t_{ij}$ is the transformation matrix from central moments to distributions as $\mathbf{f} = T\mathbf{m}$. Since cumulants and central moments are equal up to third order, one has $r_l = 0, l \in \mathcal{L}$, yielding:

$$f_i = \sum_{l \in \mathcal{L}} t_{il} k_l + \sum_{h \in \mathcal{H}} t_{ih} (k_h + r_h). \quad (7)$$

For Eq. (3), we can obtain k_h by solving

$$\frac{\partial \tilde{H}(\mathbf{f})}{\partial k_h} = 0, h \in \mathcal{H}. \quad (8)$$

The left-hand side of Eq. (8) can be evaluated as

$$\frac{\partial \tilde{H}(\mathbf{f})}{\partial k_h} = - \sum_i \frac{\partial f_i}{\partial k_h} \cdot \frac{2f_i}{\omega_i}. \quad (9)$$

Then with Eq. (7), we can rewrite Eq. (8) as

$$\sum_i \frac{\partial f_i}{\partial k_h} \cdot \frac{\sum_{h \in \mathcal{H}} t_{ih} (k_h + r_h)}{\omega_i} = - \sum_i \frac{\partial f_i}{\partial k_h} \cdot \frac{\sum_{l \in \mathcal{L}} t_{il} (k_l + r_l)}{\omega_i}, \quad (10)$$

Now, if we denote $\mathbf{r} = \{r_h, h \in \mathcal{H}\}$, an important observation is that there exists a constant matrix \underline{L} in closed form and a vector \underline{n} depending only on the known low-order cumulants such that

$$\mathbf{r} = \underline{L}\mathbf{k} + \underline{n}. \quad (11)$$

We split the matrix $T = [T_l; T_h]$, and define $\underline{D} = [\frac{\partial f_i}{\partial k_h}] = T_h(\underline{I} + \underline{L})$. Written in matrix form using \underline{I} as the identity matrix and \underline{W} as the diagonal matrix containing the lattice weights ω_i , Eq. (10) becomes:

$$\underline{D}^T \underline{W}^{-1} T_h ((\underline{I} + \underline{L})\mathbf{k} + \underline{n}) = -\underline{D}^T \underline{W}^{-1} T_l \mathbf{k}_l, \quad (12)$$

which leads to

$$(\underline{I} + \underline{L})\mathbf{k} = -(\underline{D}^T \underline{W}^{-1} T_h)^{-1} \underline{D}^T \underline{W}^{-1} T_l \mathbf{k}_l - \underline{n}. \quad (13)$$

2 NUMERICAL TESTS OF GRID CONVERGENCE

2.1 Taylor-Couette flow

We perform a 2D Taylor-Couette flow test to assess the convergence of our boundary treatment. The flow is generated between two concentric rotating circles that have different radii and angular velocities, which is sketched in Fig. 1. In our case, we set $r_1 = 0.5$, $r_2 = 1.0$ and $\Omega_1 = 1.0$, $\Omega_2 = -1.0$. The Reynolds number $Re =$

$|\Omega_2|r_2^2/\nu$ is set to 10, where ν is the kinematic viscosity. In the case of a laminar flow, there is an analytical solution for the velocity between the two circles: for a node (x, y) located between the circles, with $r = \sqrt{x^2 + y^2}$ for $r \in [r_1, r_2]$, the solution \mathbf{u}^{ref} is

$$u_x^{\text{ref}} = -(A + B/r^2)y, \quad u_y^{\text{ref}} = (A + B/r^2)x, \quad (14)$$

where A and B are constants defined as

$$A = \frac{\Omega_2 r_2^2 - \Omega_1 r_1^2}{r_2^2 - r_1^2}, \quad B = \frac{(\Omega_1 - \Omega_2)r_1^2 r_2^2}{r_2^2 - r_1^2}. \quad (15)$$

We then measure the error using relative L^2 - and L^∞ -norm errors defined respectively as

$$E_{L^2} = \sqrt{\frac{\sum_i \|\mathbf{u}(\mathbf{x}_i) - \mathbf{u}^{\text{ref}}(\mathbf{x}_i)\|_2^2}{\sum_i \|\mathbf{u}^{\text{ref}}(\mathbf{x}_i)\|_2^2}}, \quad (16)$$

$$E_{L^\infty} = \frac{\max_i \|\mathbf{u}(\mathbf{x}_i) - \mathbf{u}^{\text{ref}}(\mathbf{x}_i)\|_2}{\max_i \|\mathbf{u}^{\text{ref}}(\mathbf{x}_i)\|_2}, \quad (17)$$

where $\mathbf{u}(\mathbf{x}_i)$ is the simulated velocity at lattice node \mathbf{x}_i . The relative L^2 - and L^∞ -norm errors of our solver for the Taylor Couette flow are plotted in Fig. 2, demonstrating that the error decreases as the grid is refined with an approximately first-order convergence rate.

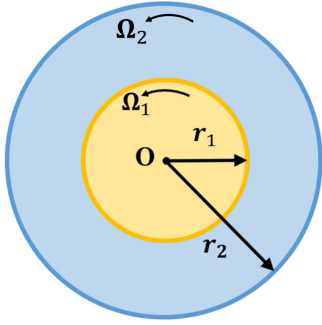


Fig. 1. **2D Taylor-Couette flow.** The flow is generated by two concentric circle boundaries with radii r_1, r_2 and angular velocities Ω_1, Ω_2 , respectively. Figure courtesy of [Lyu et al. 2021].

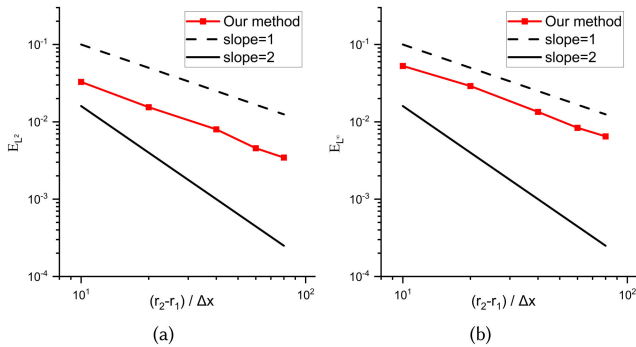


Fig. 2. **Grid convergence of Taylor-Couette flow.** We show the convergence of (a) relative L^2 and (b) relative L^∞ errors of our method.

2.2 Flow over sphere

Despite our conclusive convergence test above, one could argue that the convergence behavior of a boundary treatment scheme for a low Reynolds number flow simulation is not necessarily representative of the results for a high Reynolds number flow simulation. So we now test the accuracy of C_d evaluations for high Reynolds number flows over a sphere, and will show that second-order convergence is obtained, demonstrating that our boundary treatment method is better suited for high Reynolds number simulations. We test the convergence of our method under grid refinement in the case of the drag crisis again, for a flow passing over a sphere at $\text{Re}=400,000$ as discussed in the main paper. We use four different grid resolutions as listed in Tab. 1. The diameter of the sphere is $D=1.6m$ and the domain size is $17.6m \times 17.6m \times 17.6m$ for all grid resolutions. A convergence plot of drag coefficients as a function of $N^{-2/3}$ (where N is the total number of nodes for a given grid) is shown in Fig. 3. The plot indicates that the results computed by our method vary monotonically with grid refinement. The plot is almost linear over the three finest grids, showing a second-order convergence with respect to N . We can also see that for the coarsest grid, the drag coefficient is not decreased as expected at the drag crisis: the flow is too under-resolved in this case to capture this crisis phenomenon.

Table 1. **Test of four grids.**

No.	Δx	Node count N	$N^{-2/3} \times 10^{-6}$
1	$D/320$	42,720,181	8.18
2	$D/384$	71,695,197	5.79
3	$D/448$	108,587,682	4.39
4	$D/512$	125,631,687	3.99

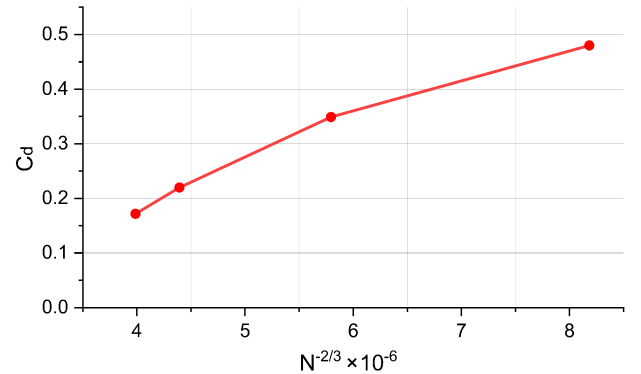


Fig. 3. **Drag estimates C_d for flow around sphere at $\text{Re} = 400,000$.**

REFERENCES

- Martin Geier, Andrea Pasquali, and Martin Schönherr. 2017. Parametrization of the Cumulant Lattice Boltzmann Method for Fourth Order Accurate Diffusion Part I: derivation and validation. *J. Comp. Phys.* 348 (2017), 862–888.
- Andreas Krämer, Dominik Wilde, Knut Küllmer, Dirk Reith, and Holger Foysi. 2019. Pseudoentropic derivation of the regularized lattice Boltzmann method. *Phys. Rev. E* 100 (2019), 023302, Issue 2.
- Chaoyang Lyu, Kai Bai, Yiheng Wu, Mathieu Desbrun, Changxi Zheng, and Xiaopei Liu. 2023. Building a Virtual Weakly-Compressible Wind Tunnel Testing Facility. *ACM Trans. Graph.* 42, 4 (2023).
- Chaoyang Lyu, Wei Li, Mathieu Desbrun, and Xiaopei Liu. 2021. Fast and Versatile Fluid-Solid Coupling for Turbulent Flow Simulation. *ACM Trans. Graph.* 40, 6, Article 201 (2021).